

2

AD-A241 782



Office of the Chief of Naval Research
Contract N00014-87-K-0326
Technical Report No. UWA/DME/TR-91/6

A BAR IMPACT TESTER FOR DYNAMIC FRACTURE TESTING
OF CERAMICS AND CERAMIC COMPOSITES



L. R. Deobald and A. S. Kobayashi

July 1991

Approved for release by NSA on 05-08-2014 pursuant to E.O. 13526

91-12857



The research reported in this technical report was made possible through support extended to the Department of Mechanical Engineering, University of Washington, by the Office of Naval Research under Contract N00014-K-0326. Reproduction in whole or in part is permitted for any purpose of the United States Government.

91 12857

A BAR IMPACT TESTER FOR DYNAMIC FRACTURE TESTING OF CERAMICS AND CERAMIC COMPOSITES

L. R. Deobald and A. S. Kobayashi
Department of Mechanical Engineering
University of Washington
Seattle, WA 98195

Abstract

A bar impact test was developed to study the dynamic fracture responses of precracked ceramic bars, Al_2O_3 and 15/29% volume $\text{SiC}_w/\text{Al}_2\text{O}_3$. Laser interferometric displacement gage data was used together with dynamic finite element analysis to determine the instantaneous crack length and the dynamic stress intensity factor, $K_I(t)$, in the fracturing ceramic bars impacted with impactor velocities of 5.8, 8.0, and 10 m/s. The crack velocities increased from 1400 to 2600 m/s with increasing impact velocity. The dynamic initiation fracture toughness and an increasing $K_I(t)$ with time and with increasing impact velocity were obtained.

1. Introduction

Available configurations of new ceramics and ceramic composites are often restricted to bar geometries of about 10 x 10 mm in cross section due to the historical precedence of using modulus of rupture (MOR) tests to determine the mechanical properties of early experimental materials. The MOR specimens are ideally suited for single-edge notched, three-point bend testing to determine fracture toughness despite the inherent experimental difficulties associated with such small specimens. The small three-point bend fracture specimens, however, are extremely sensitive to the interactions of reflected stress waves with the propagating crack tip as evidenced by the copious fluctuations in the dynamic stress intensity factor during the dynamic fracture process [1,2]. Moderate fluctuations in dynamic stress intensity factor in relatively large three-point bend specimens of 75 mm height and 10 mm thickness and 89 mm height and 9.5 mm thick were documented in [3] and [4], respectively, but not to the extent shown in [1,2]. This superfluous reflected stress wave effects was eliminated by replacing the above two-dimensional fracture specimens with an

one-dimensional specimen, such as that used by Duffy and his colleagues [5,6]. Despite its cleanness in test conditions, this split Hopkinson tensile bar test, which is loaded by explosives, requires special training and laboratory facilities. Thus a need exists for a similar clean test which can be executed without such special facilities. The objective of this paper is to describe such a dynamic fracture test procedure involving a bar impact test.

2. Bar Impact Test

The bar impact experiment consists of a 50.8 mm long, rectangular bar specimen which is impacted on its end by a 25.4 mm long bar impactor of the same material. The reflected tension wave from the free end of the specimen bar interacts with the incoming compressive wave and generates a sharp tensile stress pulse of 3.6 μ s duration in the middle of the bar specimen with the transit of approximately 3/4 of the compressive pulse as shown by the Lagrangian diagram of Fig. 1.

A schematic of the experimental apparatus is shown in Fig. 2. The specimen bar and impactor bar are held by molded urethane holders which are mounted in two carriages. Both the specimen carriage and the impactor carriage run on guide rails. An air gun propels the impactor carriage down the guide rails towards the stationary specimen carriage. The ceramic bars collide well before the collision of the urethane holders and produces compressive stress waves emanating from the impact faces. This compressive stress is proportional to the impact velocity which was measured by a laser velocity measurement system. The measured strain was used to determine the initial rise in the stress history and its relation to the LIDG signal.

The specimen geometry is shown in Fig. 3. The ceramic materials tested and the corresponding nominal mechanical properties are shown in Table 1. A sharp precrack with an approximate initial length of 3 mm was generated by the Single-edge-precracked-beam (SEPB) method [7] from a shallow chevron notch. The compressive wave passes through the sharp crack whereas the reflected tensile wave will open the crack surface and initiate dynamic crack propagation. The crack opening displacement (COD) at the location X was measured using the laser interferometric displacement gage (LIDG) system [8]. LIDG targets were mounted at the precrack tip such that the reflective indentations, 0.4 mm apart, straddled the precrack as shown in Fig. 3. Also a short strain gage of 1.6 mm gage length was mounted at the mid-length of the bar on the surface opposite to the precrack.

Unit	Serial
A-1	

3. K_{Id} Determination

The dynamic initiation fracture toughness, K_{Id} , was determined by using the solution to a stress wave impinging on a stationary crack in an infinite body [9]. The stress intensity factor of a stationary crack subjected to a square tension pulse is [10]

$$K_I(t,0) = \frac{2 \sigma_0}{(1-\nu)} \left(\frac{C_1 (1-2\nu)}{\pi} \right)^{1/2} t^{1/2}. \quad (1)$$

Experimentally, the stress was measured with a strain gage and recorded at 0.1 μ s intervals. The numerical determination of K_{Id} is a simple superposition of the discrete stress values as

$$K_{Id} = \frac{2}{(1-\nu)} \left(\frac{C_1 (1-2\nu)}{\pi} \right)^{1/2} \sum_{i=1}^n \Delta\sigma_i \Delta t_i^{1/2} \quad (2)$$

4. Dynamic Finite Element Modeling

A commercial finite element code, ABAQUS¹, was used to simulate the dynamic fracture of the impact loaded ceramic bar. Although the impact was not symmetric, the stress state and stress wave propagation becomes completely symmetric after the stress wave has propagated about the length of the bar and thus only half of the bar was modeled. Stress wave propagation is simulated in the finite element model by ramping the initial compressive stress at the impact end to zero over a 1.6 μ s duration. This creates a tension pulse propagating towards the center of the bar. As shown in Fig. 1, two tension pulses, which meet at the crack plane at the post impact time of 8.6 μ s, produce a sudden net tension stress. This tension pulse is modeled by the tension wave which reflects off of the rigid boundary along the crack plane as a tension wave in the one-half finite element model. This reflected tension wave in the finite element method (FEM) model represented the tension wave passing from the back half of the bar in a real test. The crack was then allowed to open at the time the crack plane was predicted to be in tension. After a delay of about 0.6 μ s, a constant crack velocity was then prescribed and the energy release rate, G_I , was calculated from the change in the total energy in the model as the crack propagated. The dynamic stress intensity factor, K_I , for the constant velocity crack was calculated by [9]

¹ Hibbit, Karlsson and Sorensen, Inc., Providence, RI 02906-4402 USA.

$$K_I^2(t) = \frac{2\mu C_2^2 D(V)}{V^2 \beta_1} G_I \quad (3)$$

where $C_2 = \sqrt{\mu/\rho}$ (4)

$$D(V) = 4 \beta_1 \beta_2 - (1 + \beta_2^2)^2 \quad (5)$$

$$\beta_1^2 = 1 - V^2/C_1^2 \quad \beta_2^2 = 1 - V^2/C_2^2 \quad (6)$$

$$\mu = \frac{E}{2(1+\nu)}$$

V is the crack velocity, C₁ and C₂ are the dilatational and shear wave velocities, respectively, E and μ, are the modulus of elasticity and the shear modulus, respectively, and ρ is the mass density.

5. Derivation of Ψ and Ω from Dynamic Fracture Theory

A non-dimensional parameter, Ψ, was derived by the simple inversion of the dynamic displacement equation [12] where the crack opening displacement (COD) can be represented as

$$\text{COD} = \frac{4(1+\nu)K_I}{E} \sqrt{2r/\pi} \left(\frac{\beta_1 (1-\beta_2^2)}{D(V)} \right) \hat{f}(K_I, r) \quad \text{where } r = a-X \quad (7)$$

$\hat{f}(K_I, r)$ is defined in [12], a is the crack length, and X is the distance along the crack at which the COD is determined. The non-dimension parameter, Ψ, is then defined from the above Equation (7) as

$$\Psi = (4\hat{f})^{-1} \sqrt{\pi/2} = \frac{K_I \sqrt{a-X} f(V)}{E' \text{ COD}} \quad \text{where } f(V) = \frac{\beta_1 (1-\beta_2^2)}{(1-\nu) D(V)} \quad (8)$$

For the near field asymptotic solution, $\hat{f} = 1$ and the theoretical value of Ψ becomes $\Psi_{\text{theo.}} = \sqrt{\pi/32}$.

A second non-dimensional parameter, Ω , was also derived based on an empirical relationship between the energy consumed at the crack tip and the strain energy flux into the crack tip region. Details of this derivation can be found in [12]. Again, the COD can be rewritten as

$$\text{COD} = \frac{4}{E'} \sqrt{2(a-X)/\pi} \left(\frac{\beta_1 (1-\beta_2^2)}{(1-\nu)D(V)} \right) \hat{f}(K_I, r) \left(g(V) \sqrt{\hat{k}(a-X) W} \right) \quad (9)$$

Rearranging Equation (9), the non-dimensional parameter, Ω , was defined as

$$\Omega = 4\sqrt{2/\pi} \hat{f} X \sqrt{\hat{k}/W} = \frac{X E' \text{COD}}{(a-X) W \sigma_0 f(V) g(V)} \quad (10)$$

where

$$K_I = g(V) \sqrt{\hat{k}(a-X) W} \quad g(V) = \left(\frac{C_1 C_2^2 D(V)}{2 (1+\nu) V^3 \beta_1} \right)^{1/2} \quad (11)$$

\hat{k} is a proportionality constant

The crack length history, $a(t)$, using the experimental midplane stress, $\sigma_0(t)$, was computed by the crack opening displacement, COD(t). $K_I(t)$ computation required the use of $a(t)$ and COD(t). These relations are shown in the following as functions of the two non-dimensional parameters which are referred to as calibration parameters Ω and Ψ .

$$a(t) = X \left(1 + \frac{E' \text{COD}(t)}{\Omega_c W \sigma_0(t) f(V) g(V)} \right) \quad (12)$$

$$K_I(t) = \Psi_c \frac{E' \text{COD}(t)}{f(V) \sqrt{a(t) - X}} \quad (13)$$

The crack length history, determined by Equation (12), is a function of two crack velocity dependent functions, $f(V)$ and $g(V)$. Hence, the crack length history, $a(t)$, must be determined in an iterative fashion. An initial guess was made of the crack velocity, V , to calculate $f(V)$ and $g(V)$. $a(t)$ was then calculated with Equation (12) and least squares fitted with a straight line. The slope (crack velocity) was used

to determine new estimates of $f(V)$ and $g(V)$. The process was repeated until the crack velocity converged to the correct value, which is the measured crack velocity in this case. The final value of $f(V)$ was used with $a(t)$ in Equation (13) to calculate $K_I(t)$, explicitly.

6. Determination of Calibration Constants, Ω_c and Ψ_c

The parameter, Ω , listed as Equation (10), was calculated in a series of dynamic finite element analyses for the 8.89 mm wide specimen. The crack velocities varied from 1201 to 2222 m/s. Two different initial crack lengths were included and different load levels were simulated. The results of the analyses are shown in Fig. 4. Immediately after the crack began to propagate, the non-dimensional parameter, Ω , oscillated down, and assumed a constant value. Thus Ω is not expected to yield good results near the time of crack initiation since the crack velocity jumps from zero to high constant velocities used in the simulation. From Fig. 4, a constant value of 0.95 was defined as the calibration constant, Ω_c . An additional finite element analysis of the specimen geometry with $W=7.24$ mm yielded a calibration constant of $\Omega_c=1.37$.

The calibration constant, Ω_c , was then used to determine the crack length, $a(t)$, from the measured stress history and COD history. Before using the numerically determined Ω_c , the procedure was verified by comparing the actual finite element crack history with $a(t)$ determined by the procedure presented above for $\Omega_c=0.95$. The verification is shown in Fig. 5 for four different crack velocities. Surprisingly, the large initial oscillations in the data caused little error in the predicted crack length. The error increased for two of the crack histories as the crack approached the specimen boundary.

The crack velocity correction functions, $f(V)$ and $g(V)$, are included in the parameter, Ω and thus an iterative procedure must be used to determine $a(t)$ using Equation (12). The rate of convergence of this iterative procedure was tested by using the COD and stress histories from the dynamic FEM simulation ($V=1502$ m/s) with $\Omega_c=0.95$ to predict the crack history. The crack velocity corrections functions, $f(V)$ and $g(V)$, were calculated with an initial value of $V=600$ m/s. Only four iterations were required to obtain the crack velocity of 1520 m/s which is within 1.2% of the true value.

The calibration constant, Ψ_c , was determined from a plot of the non-dimensional parameter, Ψ , shown in Fig. 6. The parameter, Ψ , was calculated from the finite element analyses for four different crack velocities. As before with Ω , the

parameter Ψ oscillated immediately after the crack velocity jumped from zero to the constant velocity. The level remained constant before dropping off slightly as the cracks passed $\alpha=a/W = 0.85$. A constant value line was fit to the data yielding the calibration constant, $\Psi_c=0.34$. This value compares well with the constant velocity crack solution in an infinite medium. When the asymptotic dynamic displacement equation is rearranged, then $\Psi_{\text{theo.}}=\sqrt{\pi/32}$. A single finite element solution was used to determine Ψ_c for the FEM model with $W=7.24$ mm. The result for the 7.24 mm wide model was $\Psi_c=0.35$ which is within 3% of Ψ_c for the 8.89 mm wide model. A speculation is made that the coarse FEM mesh causes the models to be overly stiff and the underestimated COD yielded a numerically determined Ψ_c which is slightly higher than the theoretical value, $\Psi_{\text{theo.}}$.

Again the numerically determined calibration constant, Ψ_c , was used with the FEM results to verify the method. K_I predicted using the procedure presented previously was compared with the K_I from the FEM model in Fig. 7. The large initial oscillations had only a slight effect on K_I immediately following crack initiation. The new procedure overestimated K_I beyond $\alpha=0.85$ due to the drop off shown in Fig. 6. Hence, the solution would be considered valid to about $\alpha=0.85$.

Although many finite element analyses were done to verify the data reduction technique, only one analysis was required per specimen geometry. The resulting calibration constants, Ω_c and Ψ_c , are given in Table 2 for the two geometries used here. The solution basically behaves as a constant crack velocity crack in an infinite medium. The only stress wave reflection comes from the lateral surfaces but apparently had little effect on the solution until the crack tip approached the specimen boundary.

7. Experimental Results

As mentioned previously, an accurate measurement of the impact velocity is important since it is used to calculate the stress level. Simple bar wave theory predicts a square stress pulse of magnitude $\sigma=EV_o/2C_b$ while the actual stress ramps up and oscillate around the stress level predicted by the bar wave theory as shown in Fig. 8. A typical stress pulse, which is the first compressive pulse, measured with a strain gage is also shown in Fig. 8. The reflected tension pulse will be the same shape except that the higher frequency oscillations will somewhat die out. The initial ramping at the beginning of the measured wave was combined with the maximum stress based on the measure impact velocity. This combined stress

history is shown as a shaded area in Fig. 8 and was used to calculate the experimental $a(t)$.

A typical photomultiplier tube (PMT) output of a specimen (15% vol. $\text{SiC}_w/\text{Al}_2\text{O}_3$) impacted at 8 m/s is shown in Fig. 9. The crack begins to run shortly after the arrival of the tension stress wave.

The fringe motion history shown in Fig. 9 was combined with the other PMT output to obtain the COD history for this test shown in Fig. 10. The COD data was curve fit with a higher order polynomial which was used to analyze the data at the same time increments as the stress history.

8. Crack Histories

The procedure presented previously was used to obtain the crack length histories of the ceramic specimens impacted at velocities of approximately $V_0 = 5.8, 8,$ and 10 m/s for each of the four materials. A typical crack length histories for 15% vol. $\text{SiC}_w/\text{Al}_2\text{O}_3$ are presented in Fig. 11 where the crack velocities, V , increased with increasing impact velocity, V_0 . The hot pressed alumina and the two composite materials showed nearly the same crack velocities. The 99.5% dense alumina had about a 11-31% higher crack velocity as the other three. All materials displayed a linear relationship between V and V_0 . The hot pressed alumina and the two composites showed nearly the same linear function, where as the other alumina had higher crack velocities but a smaller slope.

The initial crack lengths, a_0 , for ten of the twelve specimens were determined by observing the fracture surface with a binocular microscope. All materials exhibited a distinct fracture initiation site with the exception of the 99.5% dense alumina. On the last test of the 99.5% dense alumina, dye penetrant was baked onto the precrack area prior to testing and a_0 was determined for this specimen. The initial crack is generally curved along the crack front since the specimen is subjected to a state of plane strain in the mid section and a state of plane stress near the the side surfaces. The measured initial crack length was taken as the average distance of a_0 measured at the side surfaces and a_0 measured in the middle. The initial crack length, a_0 , is defined in Fig. 3.

9. K_I Determination

The dynamic stress intensity factor, K_I , variation for 15% volume $\text{SiC}_w/\text{Al}_2\text{O}_3$ bars impacted at three velocities each is shown in Fig. 12. The fracture toughness increased with increasing impact velocities within each material group. The K_I data

was plotted as a function of the non-dimensional crack length, $\alpha=a/W$. K_I increased rapidly to begin with, then increased more slowly as the crack approached the boundary. The increase in K_I as a function of time is even more pronounced.

Fig. 13 is a plot of K_I versus the average crack velocity, V , for all the materials in this study. The average velocity was used since the slight oscillations in the crack length curves may be due to experimental error in the analysis method.

The dynamic initiation fracture toughness, K_{Id} , was calculated by the technique presented in section 3. All results are summarized in Table 3. All specimens impacted at 10 m/s showed macroscopic crack branching. Also, the hot pressed alumina impacted at 8 m/s showed crack branching. The crack branching toughness [13], K_{Ib} , is also listed in Table 3.

The crack branching stress intensity factor, K_{Ib} , was determined by measuring the crack branch length, a_b , then choosing $K_{Ib} = K_I(\alpha=a_b/W)$ from the dynamic stress intensity factor curves e.g., Fig. 12. K_{Ib} was typically 2 to 2.5 times the magnitude of K_{Id} which is in accord with previously reported results [13]. Surpassing K_{Ib} was a necessary, but not a sufficient condition for the crack to branch and is in agreement with some tests where K_I exceeded K_{Ib} without crack branching.

10. Discussions

The basic postulate for the procedure described above is neglecting the effects of the boundaries perpendicular to the crack plane since Ψ and Ω are based on the infinite medium solution for a constant crack velocity. Both plots of Ω and Ψ displayed an initial oscillation immediately after the crack began to propagate. It is not known if these oscillations are noise associated with the numerical solution or if they indicate a real physical phenomenon.

The crack length history, $a(t)$, oscillates about a constant velocity, even when the curve fitted COD history was used. The new procedure has the limitation in that it cannot discern whether the variation in crack velocity is real or if it is experimental noise caused by stress wave reflections from the free surface in front of the crack tip. These modest oscillations in $a(t)$ were never more than 0.3 mm and seemed to have little effect on the calculation of K_I .

Before proceeding to the analysis of experimental data, it was important to verify that the numerically determined calibration constants, Ω_c and Ψ_c would determine the correct crack length history, $a(t)$ and K_I as determined by the finite element model. A verification, which used Ω_c and Ψ_c and the known stress history and COD from the FEM analysis to calculate $a(t)$ and K_I , was thus conducted. In

regard to K_I , the initial oscillation in Ψ did introduce a discrepancy of about 10% immediately after the crack began to propagate. However, K_I matched closely in the range of $0.5 < \alpha = a/W < 0.85$. The use of Ψ_c over predicted K_I above $a=0.85$ due to the drop off in the Ψ curve. The theoretical value of Ψ from the asymptotic near field solution was determined to be $\sqrt{\pi/32}$. The difference between $\Psi_{theo.}$ and Ψ may be due to an overly stiff finite element mesh. In this regard, the mesh should be significantly refined in future work.

The LIDG technique has a sensitivity of 0.911 mm for this particular setup. The experiment was such that the COD was less than 1 μm at the time the crack began to propagate. This caused uncertainty at the initial stages of the crack propagation and would have made it impossible to accurately determine a_0 or K_{I0} . Instead, a_0 was measured directly from the fracture surface and K_{I0} was calculated from the procedure presented. The crack opening displacement varied nearly linear with time. The variance from a straight line matched the time the stress wave took to propagate from the crack to the free boundary and back again.

The relationship between V_0 and V was linear, but the straight line fit did not extrapolate through the origin. The lower density alumina had higher crack velocities, but the slope was not as steep as the other materials. The crack velocities were nearly the same for the hot pressed alumina and the two composites. This was an indication that the toughening mechanisms in the composite were ineffective under this severe dynamic fracture. The higher crack velocity in the lower density alumina was in accord with other published data[1,2].

Crack propagation initiated at the respective values of K_{I0} for each material and reach values of K_I as high as 4 times K_{I0} . K_I is expected to be overestimated for $\alpha > 0.85$. K_I was calculated for the bars in which the crack branched. The K_I curve remained smooth through the branching. K_I was plotted for crack lengths greater than the crack branch length, a_b , in tests in which crack branching occurred. Although the data was plotted for $a > a_b$, the procedure has no basis for calculating K_I beyond the crack branch length, a_b . A unique relationship between V and K_I was not apparent from the results of this experiment. Other researchers have reported similar results for ceramic materials [1,2]. The uniqueness of the K_I versus V curve continues to be a source of controversy and the results of this study did not resolve this question due to the insufficient resolution in determining the crack velocity.

A great advantage of this technique was that the crack was loaded by a relatively "clean" tension stress which is uniform across the crack plane and loads

the crack in mode I opening only. The duration of the experiment was less than the time for the primary release waves to return to the crack. The potential exist for this experiment to be analyzed from dynamic fracture theory without an expensive dynamic finite element analysis. The crack behaved as a crack in an infinite solid for the limited duration of the experiment. The theory of dynamic fracture under stress wave loading would be applicable for this limited time before boundary effects become significant.

11. Conclusions

- 1) A new type of experiment was designed to study the dynamic fracture behavior of ceramic materials. The new test method provided several distinct advantages over current experimental methods.
 - A predictable and "clean", unidirectional stress pulse was suddenly applied at the crack plane.
 - A sharp precrack was introduced in the ceramic bar yielding better estimates of K_{I_d} .
 - Once set up, this experiment was relatively easy to perform and was comparable to the popular instrumented Charpy impact test.
 - The experiment was capable of producing \dot{K}_I in the range of $10^7 \text{ MPa}\sqrt{\text{m/s}}$, which surpasses the more complicated Hopkinson bar experiments.
 - The method gave consistent results for $a(t)$ and K_I .

- 2) A new method of analysis was developed for converting the measured COD and stress to useful K_I data. The technique provided the following contributions:
 - Two non-dimensional invariant parameters, Ω and Ψ were derived. The constants defined as Ω_c and Ψ_c were used to analyze any number of experiments of any material at a variety of impact velocities.
 - Only one dynamic finite element analysis was needed per specimen geometry to analyze a series of tests. This makes dynamic fracture study of ceramic materials more economical.

- 3) Dynamic fracture theory was used to determine K_{I_d} based on a measured stress wave.
- 4) The toughening mechanisms for $\text{SiC}_w/\text{Al}_2\text{O}_3$ composites were ineffective when the material was subjected to severe dynamic fracture conditions.
- 5) A unique relationship between crack velocity and K_I was not apparent for the crack velocities in the range of 1400 to 2600 m/s.
- 6) The project verified that $K_{I_b} \approx 2$ to 2.5 times K_{I_d} and that the crack velocity at which branching occurred was roughly $0.4C_2$.

12. Acknowledgement

This research was supported by the Office of Naval Research Contract No. 0004-87-K032. The authors express their sincere gratitude to Drs. Yapa Rajapakse and Steve Fishman for their patience and encouragement during the course of this investigation.

13. References

1. Yang, K.H., Kobayashi, A.S., Emery, A.F., "Dynamic Toughness of Ceramic Composites," Ceramic Engineering Science Proceedings 9(7-8) (1988) 795-802.
2. Takagi, Y. and Kobayashi, A.S., "Further Studies on Dynamic Fracture Response of Alumina and $\text{SiC}_w/\text{Al}_2\text{O}_3$ Composite," Proc. of Symp. on Elevated Temperature Crack Growth, eds. S. Mall and T. Nicholas, ASME MD-Vol. 18 (1990) 145-148.
3. Kalthoff, J.F., Winkler, S. and Beinert, J., "The Influence of Dynamic Effects in Impact Testing," International Journal of Fracture, Vol. 13, 1977, 528-531.
4. Mall, S., Kobayashi, A.S. and Urabé, Y., "Dynamic Photoelastic and Dynamic Finite Element Analyses of Dynamic Tear Test Specimens," Experimental Mechanics, Vol. 16, December 1978, 449-458.
5. Marchand, A., Duffy, J.F. Christman, T.A. and Suresh, S., "An Experimental Study of the the Dynamic Mechanical Properties of an Al- SiC_w Composite," Engineering Fracture Mechanics, Vol 30, No. 3, 1988, 295-315.

6. Suresh, S, Nakamura, T., Yeshurun, Y., Yang, K.-H. and Duffy, J.F., "Tensile Fracture Toughness of Ceramics Materials: Effects of Dynamic Loadings and Elevated Temperature," *Journal of American Ceramic Society*, Vol 73, No. 8, 1990, 2457-2466.
7. Nose, T. and Fujii, T., "Evaluation of Fracture Toughness for Ceramic Materials by a Single-Edge-Pre-cracked-Beam Method." *J. of the Amer. Cer. Soc.*, **71** (5) (1988) 328-333.
8. Sharpe, W.N., Jr., "A New Optical Technique for Rapid Determination of Creep and Fatigue Thresholds at High Temperatures," AFWAL TR 84-4028, Air Force Wright Aeronautical Laboratories, WPAFB, 1984.
9. Freund, L.B., "Crack Propagation in an Elastic Solid Subjected to General Loading-III. Stress Wave Loading," *J. Mech. Phys. Solids*, **21** (1973) 47-61.
10. Ravichandran, G. and Clifton, R.J., "Dynamic Fracture Under Plane Wave Loading," Brown University Report No. AD-A178 594.
11. Nishioka, T. and Atluri, S.N., "Path-Independent Integrals, Energy Release Rates, and General Solutions of Near-Tip Fields in Mixed-Mode Dynamic Fracture Mechanics." *Eng. Fracture Mechanics*, **18** (1) (1983) 1-22.
12. Deobald, L. R., "Numerical/Experimental Characterization of the Dynamic Fracture Behavior of Ceramic Materials," a Ph.D. thesis submitted to University of Washington, June 1991.
13. Ramulu, R. and Kobayashi, A.S., "Mechanics of Crack Curving and Branching," *Int'l J. of Fracture*, **27** (1985) 187-201.

ASK/cm/ONR/TR91/7-24-91

Table 1. Mechanical properties

Materials	E (GPa)	ν	ρ (g/cc)	C_1 (mm/ μ s)
Al ₂ O ₃ ¹ 99.5%	372	.22	3.89	9.78
Al ₂ O ₃ ² 99.9% —HP ³	387	.22	3.97	9.87
15% v SiC _w /Al ₂ O ₃ ² —HP	398	.23	3.85	10.17
29% v SiC _w /Al ₂ O ₃ ² —HP	408	.23	3.73	10.46

C_1 is the dilatational wave velocity

Table 2. Calibration constants, Ω_c and Ψ_c , calculated by FEM.

W (mm)	X (mm)	Ω_c	Ψ_c	$\Psi_{theo.}$
8.89	2.5	0.95	0.34	0.313
7.24		1.37	0.35	

¹ Coors Ceramic Company, 600 9th Street, Golden, CO 80401 USA.

² Advanced Composite Materials Corporation, 1525 S. Buncombe Road, Greer, SC 29651 USA.

³ Hot pressed processing.

Table 3. Experiment Summary

Material	V_0 m/s	V m/s	V/C_2	K_{IC} MPa√m	K_{Id} MPa√m	K_{Ib} MPa√m
Al ₂ O ₃	5.8	1975	0.32	3 - 4	5.3	-
	7.9	2317	0.37		5.9	-
	10.3	2605	0.42		5.2	12.4
Hot Pressed Al ₂ O ₃	5.7	1546	0.24	4	5.9	-
	8.1	1830	0.29		6.8	14.9
	10.1	2465	0.39		5.8	13.6
15% vol. SiC _w /Al ₂ O ₃	5.8	1457	0.22	6	9.0	-
	8.0	1872	0.29		6.5	-
	10.0	2210	0.34		6.7	14.2
29% vol. SiC _w /Al ₂ O ₃	5.8	1536	0.23	7	6.5	-
	8.0	2383	0.36		5.7	-
	10.1	2383	0.36		9.8	14.2

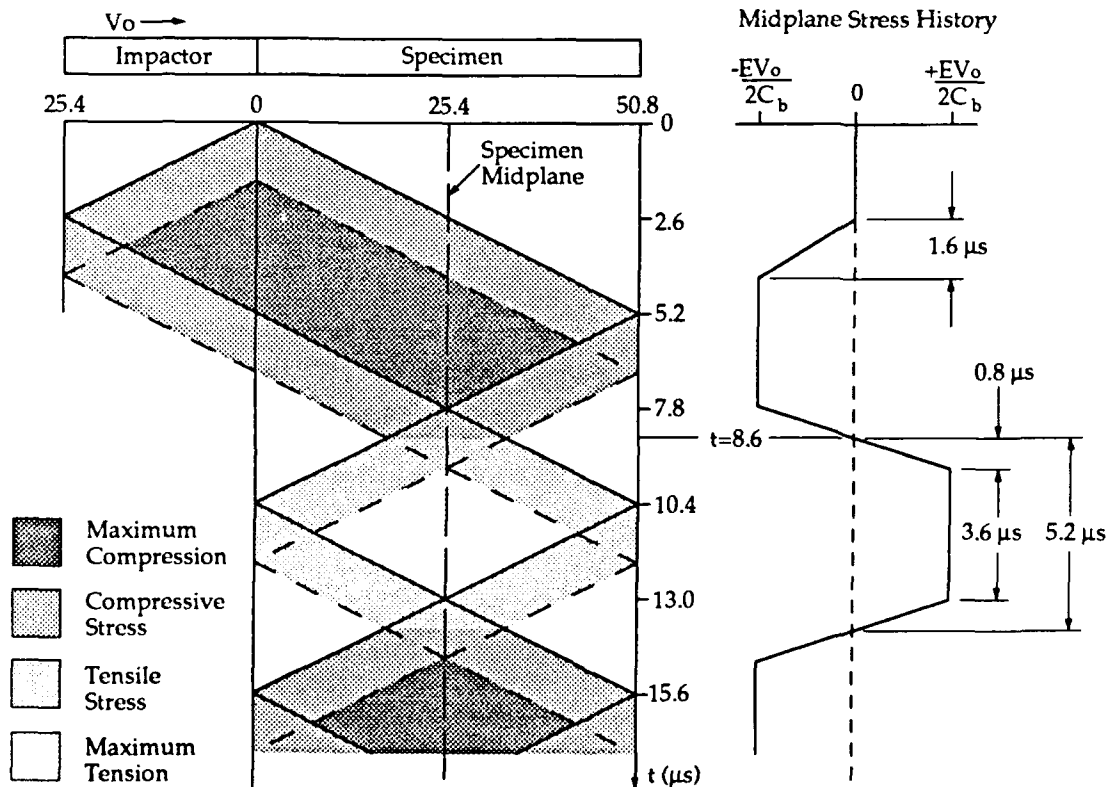


Figure 1 Lagrangian diagram for bar impact experiment.

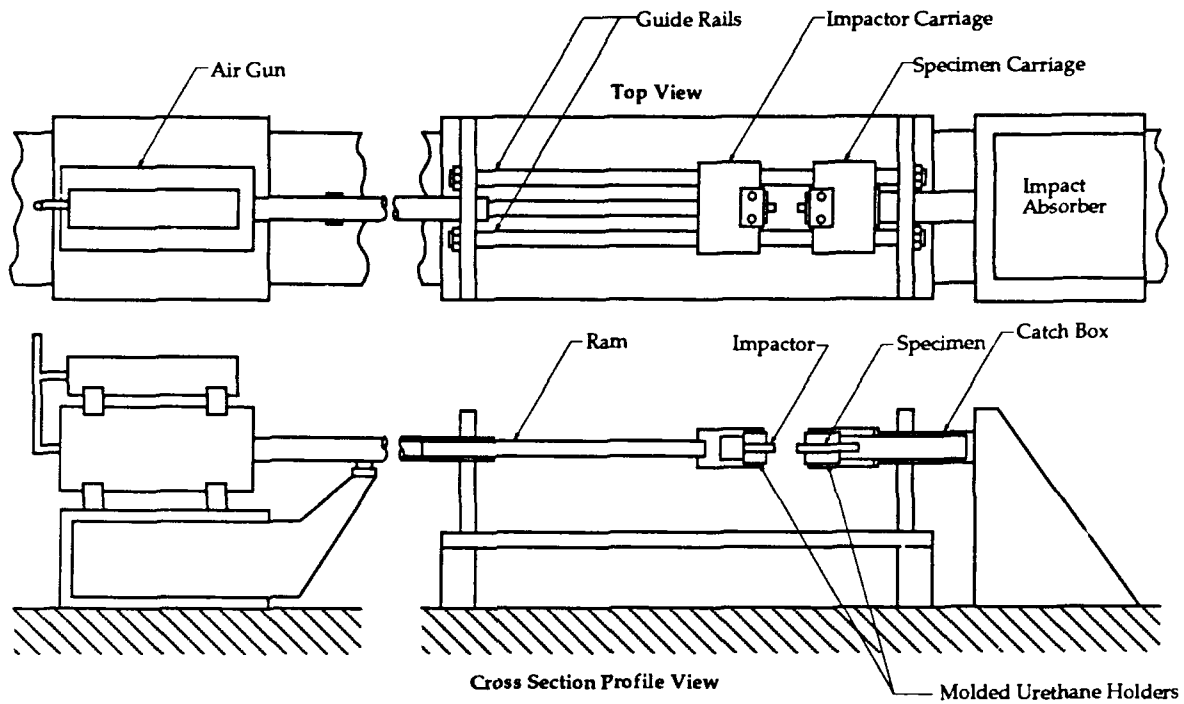


Figure 2 Impact apparatus and air gun.

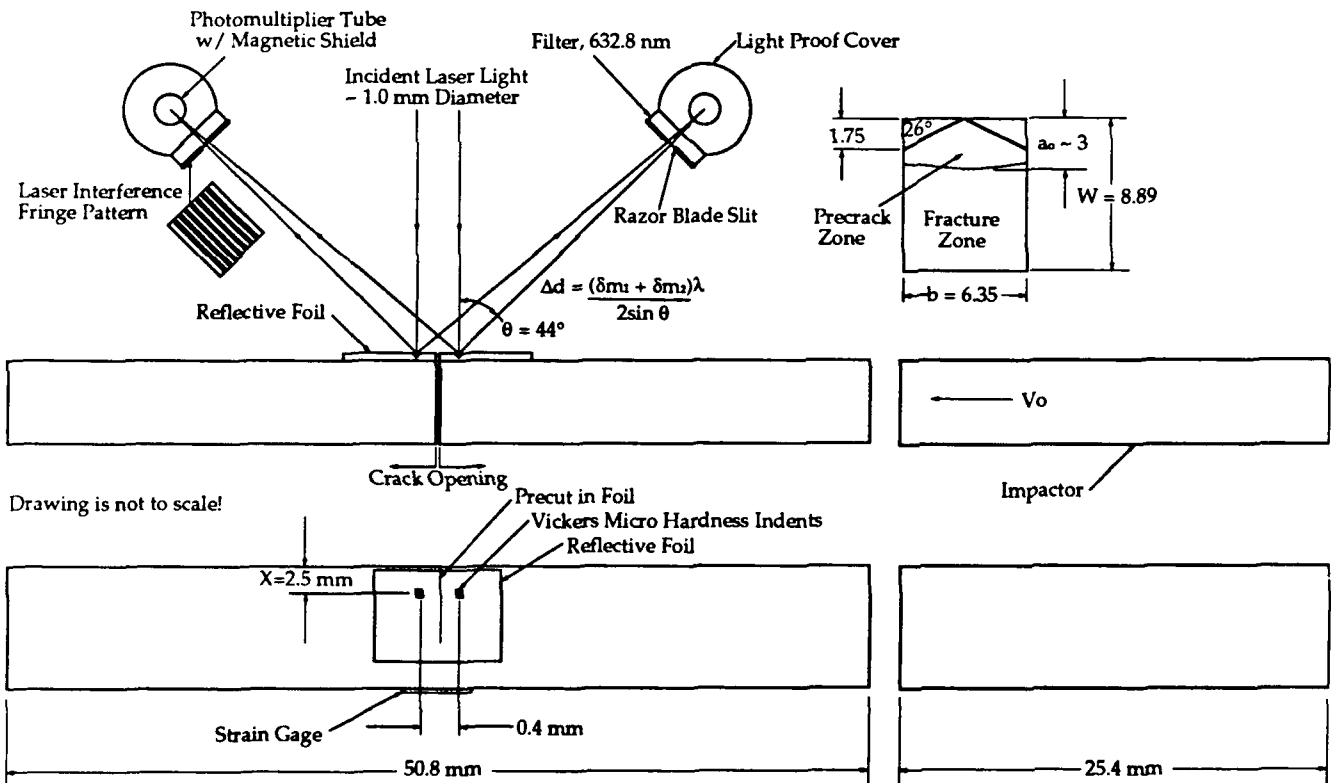


Figure 3 Specimen geometry and LIDG technique.

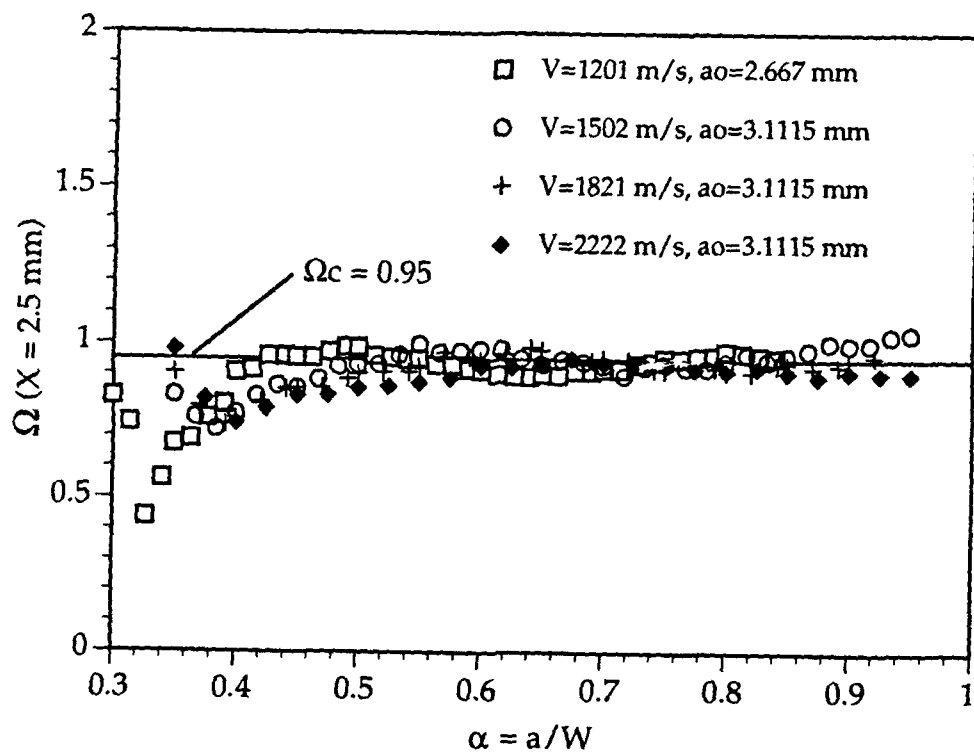


Figure 4 Finite element values of Ω vs. crack tip location, $W=8.89$ mm.

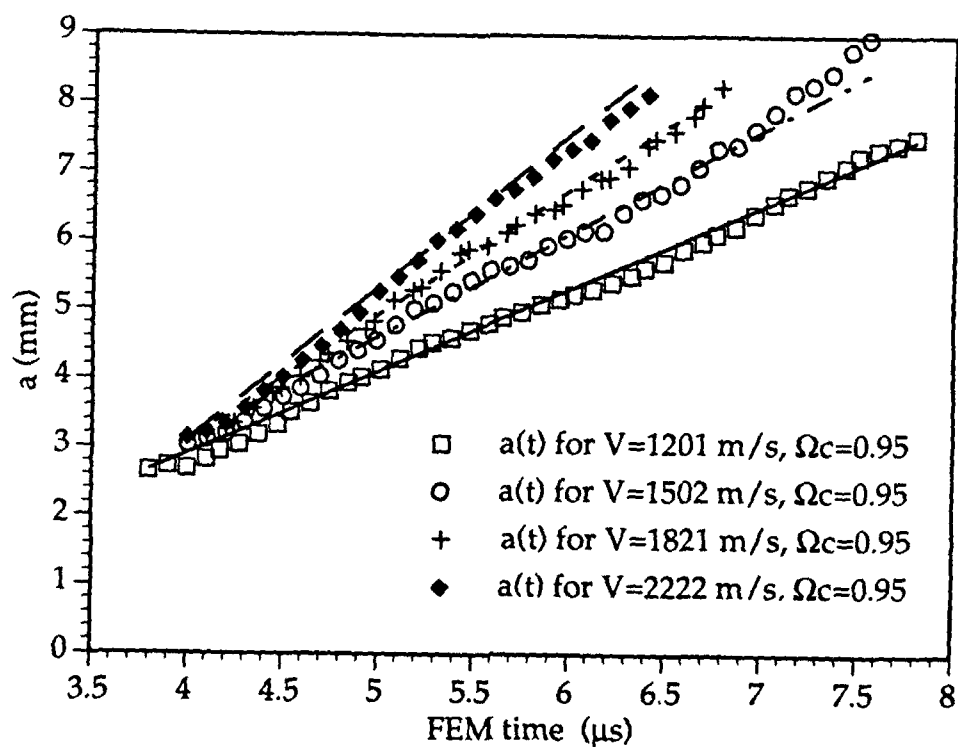


Figure 5 Finite element verification of $a(t)$, $W=8.89$ mm.

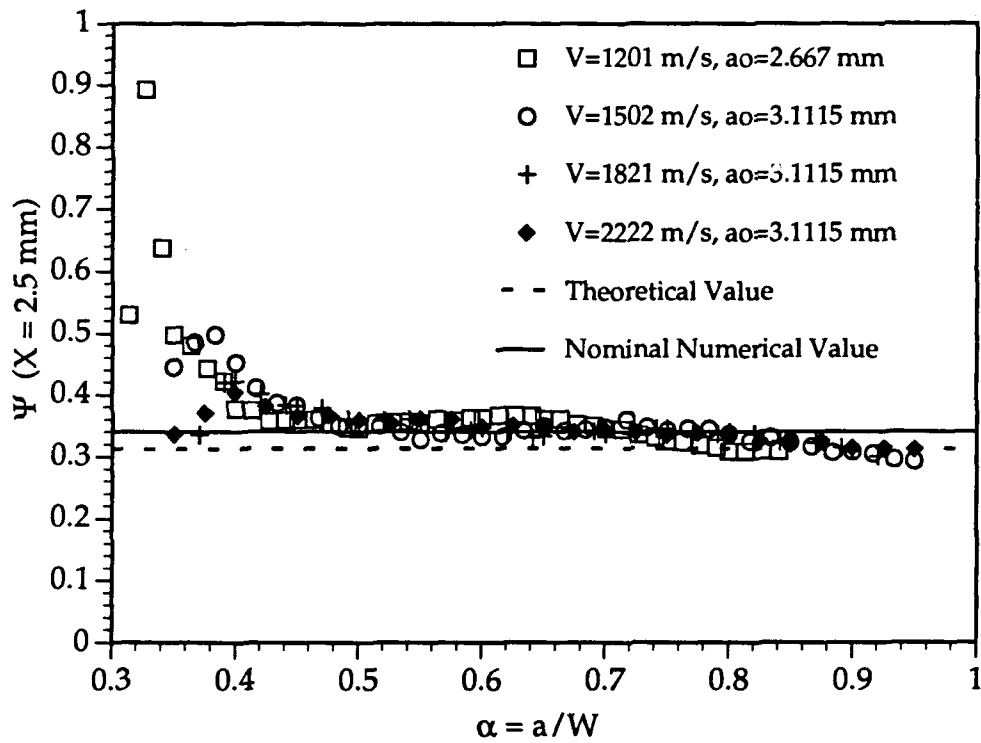


Figure 6 Finite element values of Ψ vs. crack tip location, $W=8.89 \text{ mm}$.

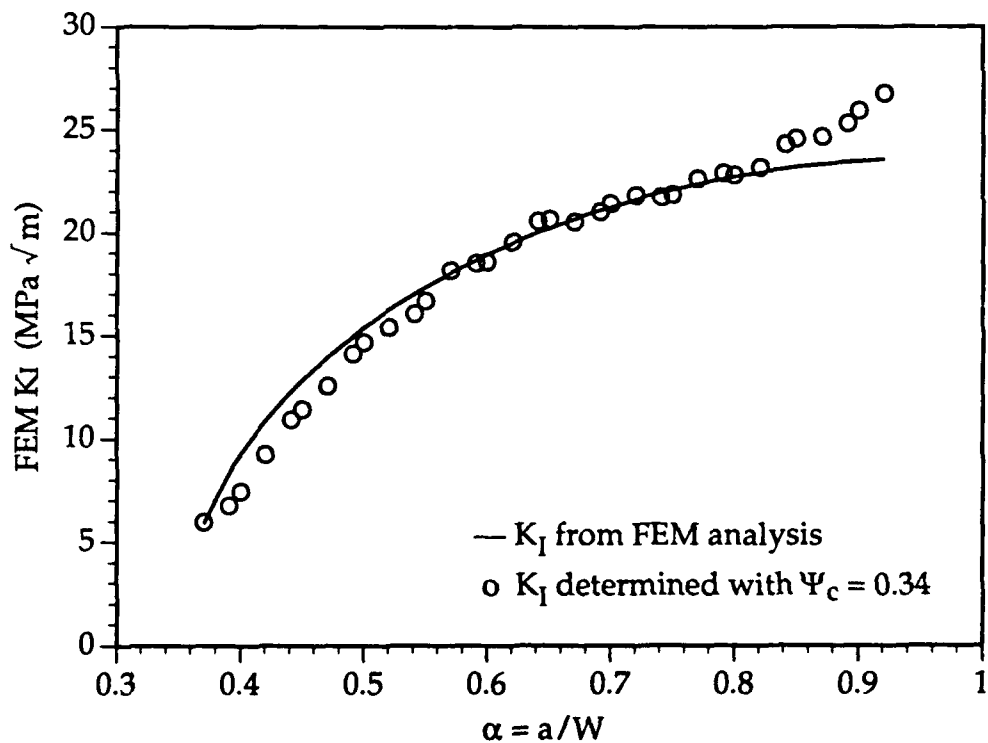


Figure 7 Finite element verification of $K_I(t)$, $W=8.89 \text{ mm}$.

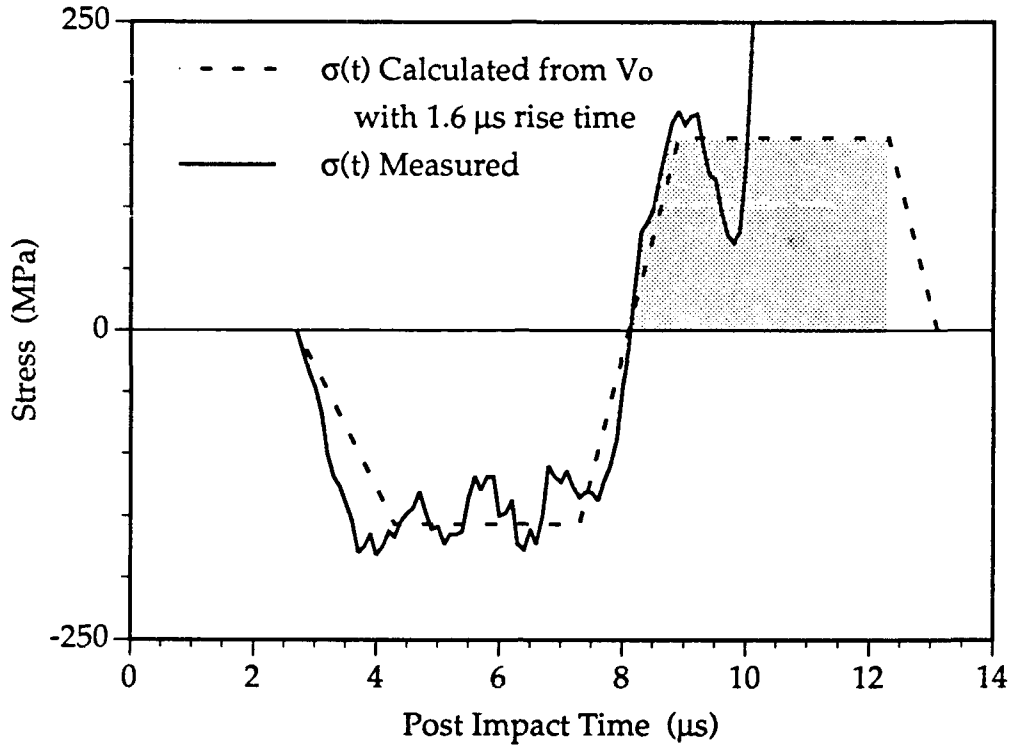


Figure 8 Typical measured stress and ideal stress.

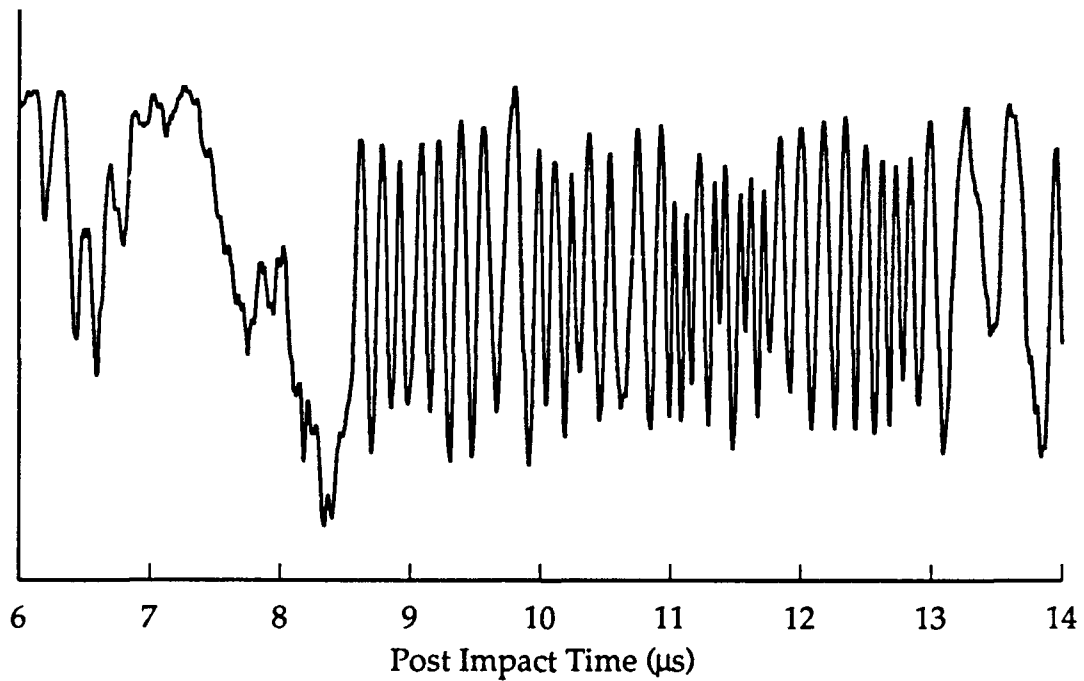


Figure 9 Typical signal representing LIDG fringe motion.

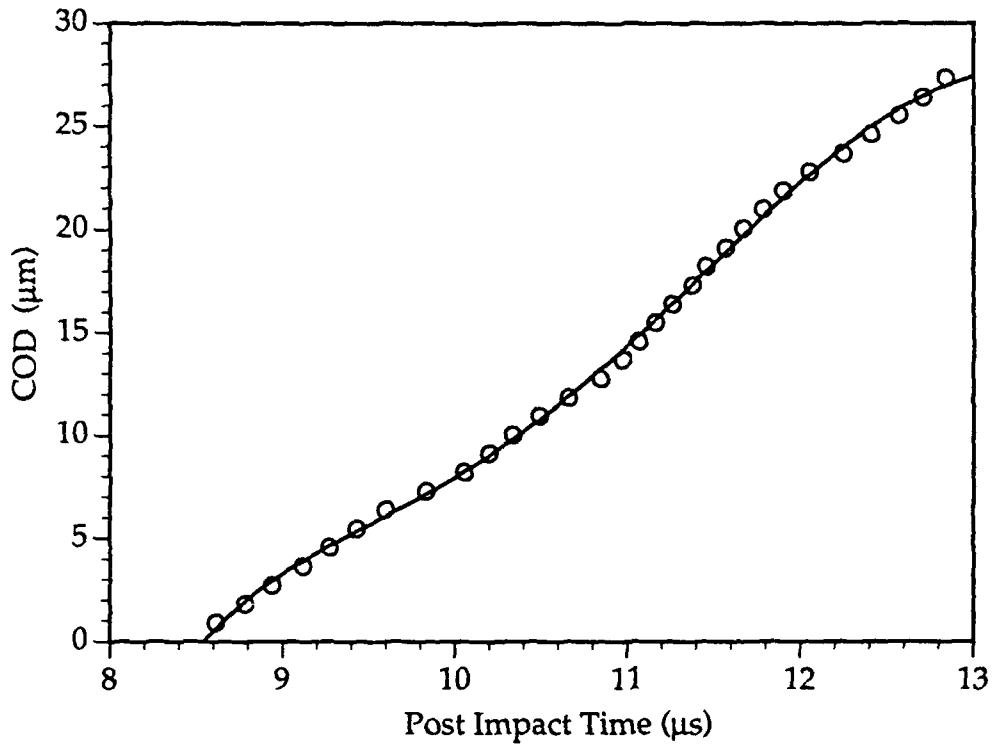


Figure 10 Typical COD history, $V_o=8$ m/s, 15% vol. $\text{SiC}_w/\text{Al}_2\text{O}_3$.

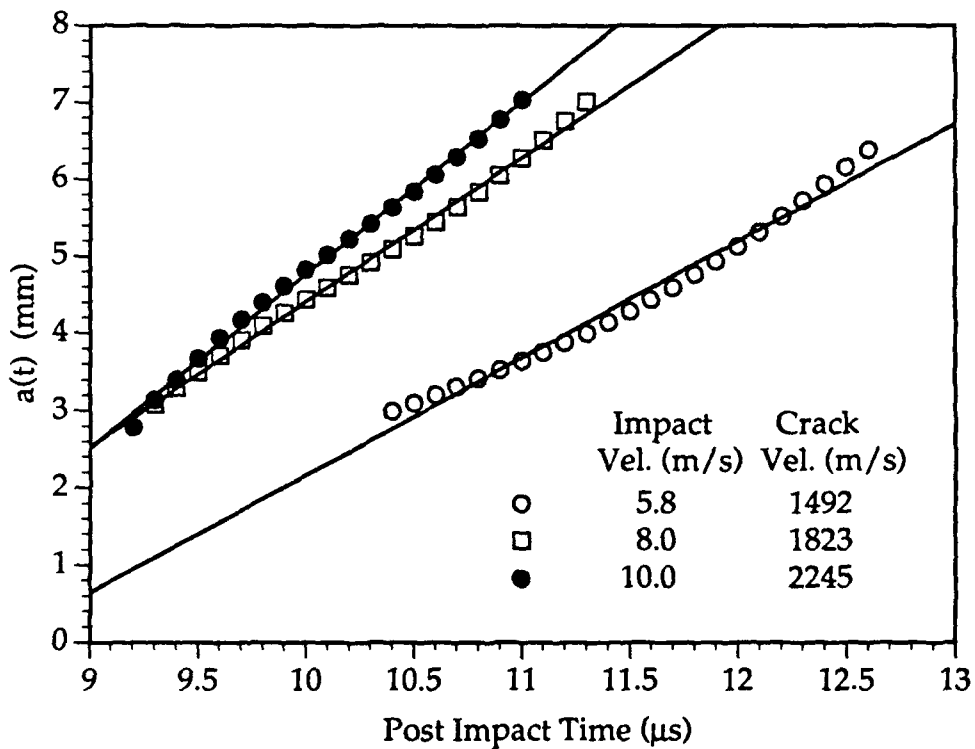


Figure 11 Typical crack length histories, 15% vol. $\text{SiC}_w/\text{Al}_2\text{O}_3$.

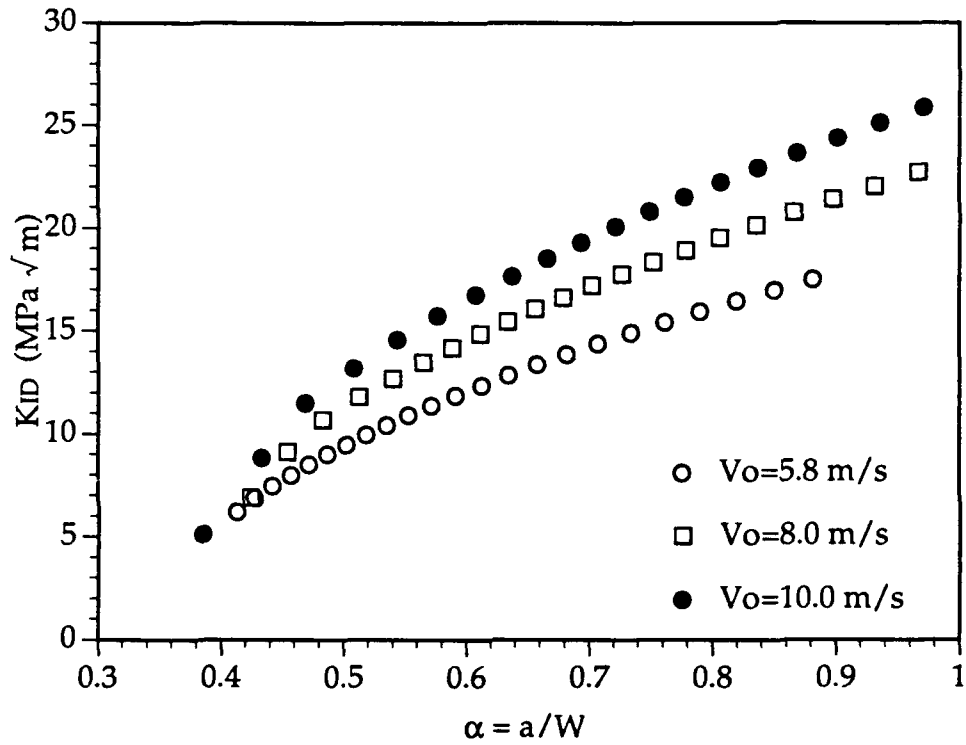


Figure 12 K_I versus α for 15% vol. $\text{SiC}_w/\text{Al}_2\text{O}_3$.

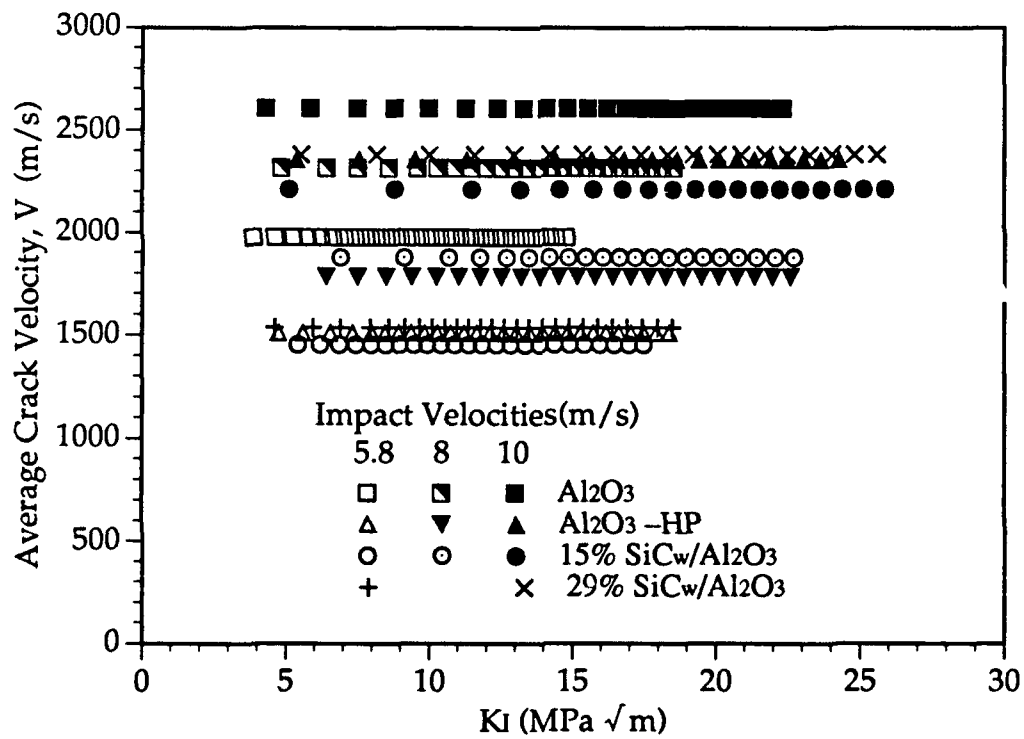


Figure 13 K_I versus average crack velocity for all materials.

REPORT DOCUMENTATION PAGE

Form Approved
OMB No. 0704-0188

Public reporting burden for this collection of information is estimated to average 1 hour per response, including the time for reviewing instructions, searching existing data sources, gathering and maintaining the data needed, and completing and reviewing the collection of information. Send comments regarding this burden estimate or any other aspect of this collection of information, including suggestions for reducing this burden, to Washington Headquarters Services, Directorate for Information Operations and Reports, 1215 Jefferson Davis Highway, Suite 1204, Arlington, VA 22202-4302, and to the Office of Management and Budget, Paperwork Reduction Project (0704-0188), Washington, DC 20503.

1. AGENCY USE ONLY (Leave blank)		2. REPORT DATE July 1991	3. REPORT TYPE AND DATES COVERED Technical Report 89-91	
4. TITLE AND SUBTITLE A Bar Impact Tester for Dynamic Fracture Testing of Ceramics and Ceramic Composites			5. FUNDING NUMBERS s400050srh05/27	
6. AUTHOR(S) L. R. Deobald and A.S. Kobayashi				
7. PERFORMING ORGANIZATION NAME(S) AND ADDRESS(ES) Department of Mechanical Engineering, FU-10 University of Washington Seattle, WA 98195			8. PERFORMING ORGANIZATION REPORT NUMBER UWA/DME/TR-91/6	
9. SPONSORING / MONITORING AGENCY NAME(S) AND ADDRESS(ES) Office of Naval Research Arlington, VA 22217-5000			10. SPONSORING / MONITORING AGENCY REPORT NUMBER	
11. SUPPLEMENTARY NOTES				
12a. DISTRIBUTION / AVAILABILITY STATEMENT Unlimited			12b. DISTRIBUTION CODE	
13. ABSTRACT (Maximum 200 words) A bar impact test was developed to study the dynamic fracture responses of precracked ceramic bars, Al ₂ O ₃ and 15/29% volume SiC _w /Al ₂ O ₃ . Laser interferometric displacement gage data was used together with dynamic finite element analysis to determine the instantaneous crack length and the dynamic stress intensity factor, K _{1D} (t), in the fracturing ceramic bars impacted with impactor velocities of 5.8, 8.0, and 10 m/s. The crack velocities increased from 1400 to 2600 m/s with increasing impact velocity. K _{1D} (t) initiated at the expected dynamic fracture toughness and increased with time and with increasing impact velocity. The dynamic initiation fracture toughness and an increasing K _{1D} (t) with time and increasing impact velocity were obtained.				
14. SUBJECT TERMS Impact, dynamic fracture			15. NUMBER OF PAGES 22	
			16. PRICE CODE	
17. SECURITY CLASSIFICATION OF REPORT Unclassified	18. SECURITY CLASSIFICATION OF THIS PAGE Unclassified	19. SECURITY CLASSIFICATION OF ABSTRACT Unclassified	20. LIMITATION OF ABSTRACT None	